Available online at www.sciencedirect.com

ScienceDirect

Ceramics International 40 (2014) 3453–3460

CERAMICS INTERNATIONAL

www.elsevier.com/locate/ceramint

Synthesis and investigation of Indium doping and surfactant on the morphological, optical and UV/Vis photocatalytic properties of ZnO nanostructure

Mehdi Rezapour*, Nasrin Talebian

Faculty of Science, Department of Chemistry, Chemistry Society, Shahreza Branch, Islamic Azad University, Isfahan, Iran

Received 25 July 2013; received in revised form 10 September 2013; accepted 20 September 2013
Available online 25 September 2013

Abstract

ZnO and Indium doped ZnO nanostructures with different morphologies have been synthesized by mild solvothermal method in the presence of cetyltrimethylammonium bromide (CTAB), sodium dodecylsulfate (SDS) and Tritron X-100 as cationic, anionic and nonionic surfactants, respectively. The hydrothermal growth mechanism was influenced by Indium impurity and surfactant. Hexagonal, flower, polyhedral and nearly spherical morphologies of ZnO were obtained. The products were characterized by X-ray diffraction (XRD), field emission scanning electron microscopy (FESEM) and transmission electron microscopy (TEM) methods. The role of surfactant charge on the ZnO growth orientation was investigated and related mechanism discussed. The highest degradation rate constant was observed for In doped flower-like ZnO synthesized using CTAB. The effects of In doping and surfactant charge on the structure, morphology, optical properties and photocatalytic activity (PCA) of ZnO nanostructures were investigated and discussed in detail. Obtained results can be utilized in the synthesis of ZnO NSs with desired growth orientation and consequently enhanced properties.

Keywords: ZnO; Dopant; Nanostructure; Photocatalysis; Surfactant

1. Introduction

Among all the metal oxide nanostructures, ZnO with wide and direct band gap and large exciton binding energy has received more attention due to different ranges of morphologies and various important properties that can be tailored by nanoscale morphologies, coupling with other semiconductors, metal doping and multilayer coating [1–5]. ZnO has the hexagonal close packed lattice with empty octahedral sites [6]. Hence, there are plenty of sites for ZnO that can be accommodated by the intrinsic defects and extrinsic dopants. It is well known that doping of ZnO with selective elements offers an effective method to adjust the electrical, optical, magnetic and catalytic properties, which is important for applications. Among all the common dopant elements, Indium is unique, because induces some structural defects that forms different morphologies and also is an efficient donor species for ZnO [7,8].

Today, one of the challenges in the ZnO related research field is improving properties through controlling the morphology and growth orientations. Polyelectrolytes [9], polymers [10], anions [11], surfactants [12] or amines [13] have been used as structure-directing agents for the synthesis of ZnO nanostructures (NSs) via the solvothermal method as an important chemical based synthesis route. High surface energy makes inorganic NSs extremely unstable, chemical reactions with the environment and also to self-aggregate of nanoparticles tend to surface energy reduction. Properties of NSs are size and shape dependent. These features of inorganic NSs mostly depend on the conditions of synthesis that create enormous difficulties in their fabrication and application. One of the most efficient ways to overcome such problems is surfactant-assisted fabrication of inorganic NSs. Over last two decades, surfactant science has made much progress in developing novel methodologies for synthesis of a great

*Corresponding author. Tel.: +98 3213292260; fax: +98 3213232701.
E-mail address: rezapoor.mehdi@yahoo.com (M. Rezapour).

0272-8842/$ - see front matter © 2013 Elsevier Ltd and Techna Group S.r.l. All rights reserved.
http://dx.doi.org/10.1016/j.ceramint.2013.09.085

variety of NSs with controlled size and well-defined morphology. Different surfactants show different impacts on the ZnO formation during synthesis, due to its structural characteristics. Understanding about special features of surfactant that influence on the ZnO growth while synthesis can help us to predict the surfactant manner while reaction, in order to manipulating the material properties. In this work cationic, anionic and nonionic surfactants have been used for synthesis and effect of surfactant charge on the ZnO formation and its properties have been investigated.

ZnO has been widely used in optoelectronics [14], different sensor devices [6], dye sensitized solar cells [15] and also has been applied as photocatalyst for the hydrogen production [16], decomposition of organic pollutants [1] and also antibacterial agent [17]. One of the major challenges in photocatalysis research area is improvement the catalyst activity in the visible light, which possesses both the chemical stability and high activity, because of its convenience and safety. In order to extend the absorption of ZnO to visible light, some kinds of modification approaches such as noble or transition metal doping [4,18], oxynitride or nitrogen doping [19] and using hybrid semiconductor systems [3] have been proposed. Total surface area of catalyst plays an important role in the capability of photodegradation, by inhibiting photogenerated electrons–holes recombination and increasing contact of species in media. The surface modification can be achieved through improving morphology [1], defects of crystal structure [1] and chemical compositions [4].

In this work, Indium doping and surfactant were used for band gap manipulation and surface characteristic modification of ZnO respectively. In spite of previous studies on preparation and effects of dopants and surfactants, certain dopants like In or evaluation of surfactant charge on the properties of ZnO, are still remaining unclear. Herein, we report the effect of both In doping and surfactant charge on the morphological, structural, optical and photocatalytic activity (PCA) of ZnO NSs under UV and Vis. irradiations. 2,4,6-trichlorophenol (TCP) was chosen as a model pollutant for evaluation the PCA of products. TCP commonly is used as pesticides, herbicides, wood preservatives and defoliants [20]. Because of its high toxicity, carcinogenic properties and structural stabilization in the environment, the destruction of TCP has been concerned so much [21].

2. Experimental

All chemicals were analytical grade and used as received without further purification. $InCl_3 \cdot 4H_2O$ was purchased from Sigma-Aldrich Co. and all other chemicals were purchased from Merck Co.

2.1. Synthesis

The ZnO and In doped ZnO NSs were synthesized via the solvothermal synthesis method in an autoclave. In first step, five 0.35 M zinc acetate dihydrate ethanolic solution were prepared and labeled as 1, 2, 3, 4 and 5. Then, $InCl_3 \cdot 4H_2O$ was added into the all solutions except number 1. The molar ratio of $InCl_3.4H_2O/Zn(CH_3COO)_2 \cdot 2H_2O$ was kept constant at 0.05. CTAB, SDS and Tritron X-100 surfactants were added to the solutions number 3, 4 and 5, respectively. The molar ratio of surfactant/Zn was kept constant at 0.05. Subsequently, 4.00 ml HCl was added drop by drop to all solutions. After stirring for 40 min at 70 °C, each prepared solution was transferred into individual cleaned stainless steel autoclave. The autoclaves were sealed and maintained in an electric oven at 170 °C for 17 h. Then, the autoclaves were cooled to room temperature. The resulting white powders were collected from the bottom of the Teflon container after decanting the supernatant. Finally, the products were washed with distilled deionized water and absolute ethanol several times and dried in vacuum oven for 5 h at 90 °C. The samples were abbreviated as follow: undoped sample as ZnO, In doped samples as IZO and In doped samples synthesized using CTAB, SDS and Tritron X-100 as IZO_C, IZO_S and IZO_T, respectively.

2.2. Characterization

To characterize the ZnO products, X-ray diffraction (XRD) were performed on a Bruker, D8 Advance XRD diffraction spectrometer with a Cu Kα line at 1.5406 Å and a Ni filter. Field emission scanning electron microscopy (FESEM) was done on a Cu-Kα, Philips, JEOL 6340 microscope, in order to investigate the morphology. Transmission electron microscopy (TEM) was carried out on a LEO system 912 AB. Particle size analysis on catalysts has been carried out for many years as the most direct way to predict the effective surface area available for catalytic activity [22]. SEM and specially TEM methods, provide particle size analysis from individual particles observed in a micrograph. The technique gives localized size information from the areas of sample where the images are obtained. The counting can be carried out one by one manually, or on a large scale by digital particle size analysis. The results are number-averaged rather than volume-averaged. Photoluminescence (PL) measurement was done using Perkinelmer LS55 photoluminescence spectrophotometer at room temperature with a Xe lamp as the excitation light source. UV-Vis absorption measurements and TCP photodegradation monitoring were performed on a Shimadzu, MPC-2200 UV-Vis spectrophotometer.

2.3. Photocatalytic experiments

ZnO powders (0.50 g L^{-1}) was suspended in an aqueous TCP solution (50.00 ppm) at normal pH. The mixture was stirred for 15 min in the absence of light to attain equilibrium adsorption on the surface of the catalyst. Four 8 W UV lamps (Philips UV-C) were supplied as the UV source and a 500 W halogen lamp as the visible light source. In the latter case, a cutoff filter was applied to ensure that irradiation is completely in the visible region. The distance between light source and solution was kept 12 cm. Degradation process was monitored through measuring the TCP concentration at λ_{max} in each degraded solution by UV-Vis spectrophotometer.

3. Results and discussions

3.1. Structural properties

Fig. 1 shows XRD patterns of ZnO, IZO, IZO_C, IZO_S and IZO_T photocatalysts. All the diffraction peaks can be well indexed to the hexagonal phase ZnO with a wurtzite structure (hexagonal phase, space group P63mc) reported in JCPDS card (No. 36-1451) [23]. The diffractograms of all ZnO samples show three characteristic diffraction peaks related to the $(10\bar{1}0)$, (0002) and $(10\bar{1}0)$ planes. To study the doping effects on the crystallinity of the ZnO NSs, the intensity and position of the $(10\bar{1}0)$, (0002) and $(10\bar{1}0)$ diffraction peaks were monitored in detail (Fig. 2). In IZO samples, the intensity of peaks was decreased considerably and the peaks position was shifted slightly toward the lower angle side. Also, The lattice parameter *c* value for the IZO NSs was increased slightly (0.5198 nm to 0.5288 nm for IZO samples). These can be attributed to the loss of crystallinity. The radius of In^{3+} and Zn^{2+} in the ZnO crystal is expected to be 76 pm and 74 pm, respectively [24]. Therefore, difference between charge density of In and Zn deforms significantly ZnO lattice. The peaks position shift, decreasing intensity of peaks and increase in lattice constant are related to the lattice expansion due to larger radius of In. Diffusion of Indium into ZnO lattice induces high activation energy; this fact suggests that there is a different diffusion mechanism involved. Therefore it is assumed that In ions occupy substitution lattice sites. Furthermore, since In ions cause increase of conductivity; consequently it cannot enter the lattice accompanied by a compensating zinc vacancy [25].

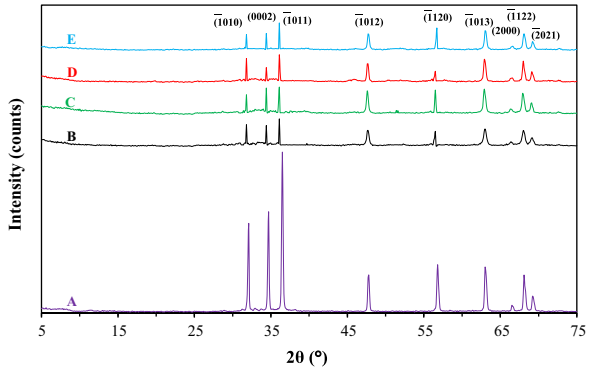

Fig. 1. XRD patterns of (A) ZnO, (B) IZO, (C) IZO_C, (D) IZO_S and (E) IZO_T.

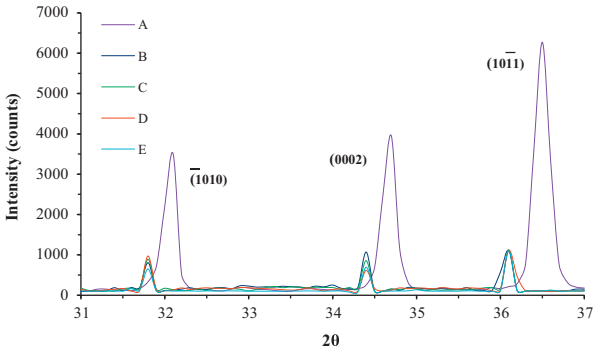

Fig. 2. XRD patterns of (A) ZnO, (B) IZO, (C) IZO_C, (D) IZO_S and (E) IZO_T in the 31–37 2θ range.

FESEM and TEM images of ZnO NSs were shown in Figs. 3 and 4 respectively. It is clear that morphologies of ZnO NSs were affected considerably by the both In doping and surfactant type. Undoped ZnO, IZO_S and IZO_T show hexagonal shape with flat planes, nearly spherical and polyhedral shape, respectively. IZO and IZO_C also showe spindle-like tapered with flower-like architecture.

The four most common terminated facets of wurtzite ZnO, are the polar Zn terminated (0002) rich in zinc and O terminated (0002) rich in oxygen, and also the nonpolar $(10\bar{2}0)$, $(10\bar{1}0)$ facets which both contain an equal number of Zn and O atoms [26]. Various properties of ZnO like surface electronic structure, chemical stability and catalytic properties depend on its polarity. For instance photocorrosion of ZnO under UV irradiation that often results in decreasing PCA in aqueous solution depends on the crystal facet [27]. For ZnO, the growth of the crystal is preferentially in the *c*-axis (0002). However the morphology, preferred growth orientation and aspect ratio, change with reaction media. This may be resulted from two interactions (1) the kinetically growth control of the certain crystal surfaces under different surfactants and (2) the electrostatic interaction between the positively charged (0002) facet of the ZnO crystal and charged chemical species. Thus surfactants can influence on the nucleation of the ZnO crystals as well as the preferential direction of crystal growth. According to latter interaction mechanism, similar molecular charge of CTAB as cationic surfactant and the (0002) plane, cause repulsion on the related plane boundary. So, for reaching more stabilization on the *c*-plane, the growth along the (0002) direction increases, resulting to spindle-like tapered with flower-like architecture. On the contrary, the negatively charged SDS molecules cause adsorption on the *c*-plane. Such interaction tends to energy on the *c*-plane decreases, so compression on the crystal in (0002) direction occurs, resulting to nearly spherical NSs. In the absence of electrostatic interaction when using Tritron X-100 as nonionic surfactant, the crystal can be grown in almost all main facets, so polyhedral morphology results. In fact, Tritron X-100 decreases media interactions around the crystal facets and allows planes to growth. Synthesized undoped ZnO shows the hexagonal shape with growth along the *m*-plane direction, whereas IZO shows the flower-like shape with growth along the *c*-plane direction. Probably incorporation of In ions into the (0002) plane lead to increasing the energy of facet, resulting instability as well. So for reaching more stability, growth along this direction occurs. Existence of surfactant in the synthesis media can alter the surface energies of various crystallographic planes to promote selective anisotropic growth of nanocrystals through adsorption. The same charge of preferred growth plane and surfactant lead to repulsion on the surface. Therefore the surface energy of related plane increase and growth along this direction increase as well, in order to reaching stabilization on the surface. Thus flower-like IZO_C in the presence of CTAB contains longer spindles then IZO. Table 1 shows the aspect

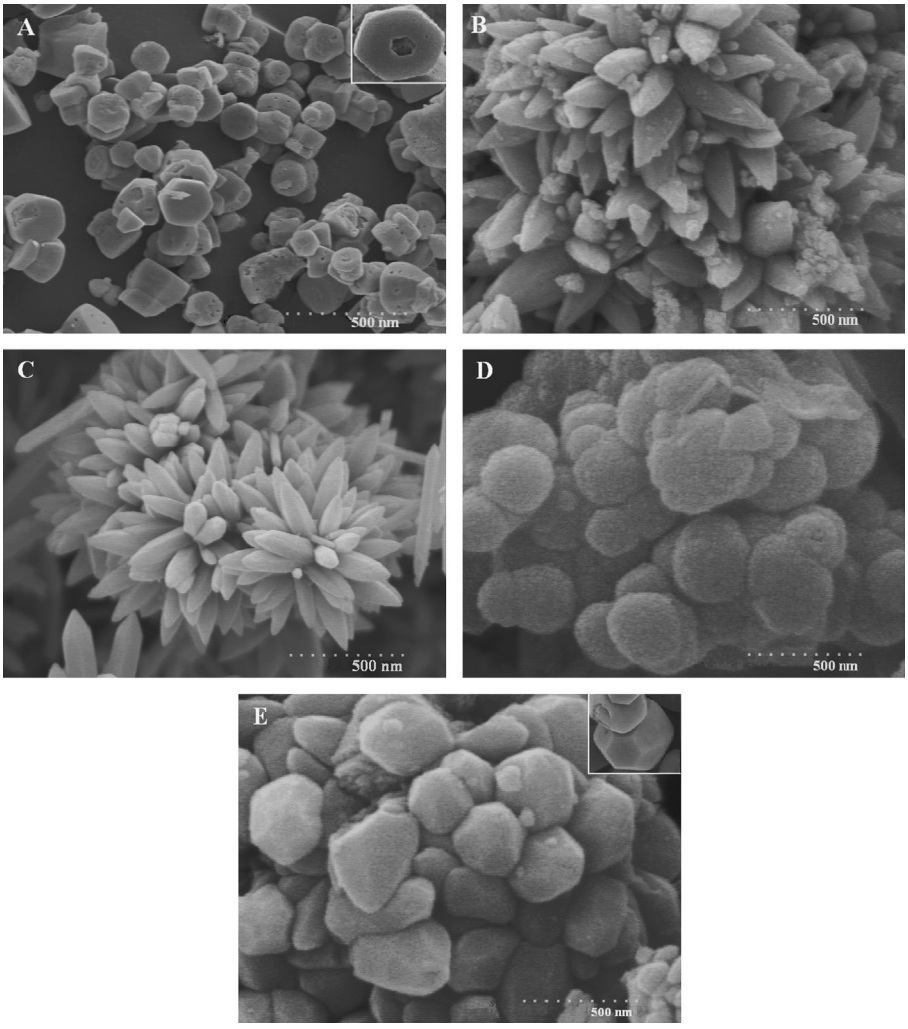

Fig. 3. SEM images of (A) ZnO, (B) IZO, (C) IZO_C, (D) IZO_S and (E) IZO_T.

ratio of the (0002)/(10$\bar{1}$1) planes obtained from both the FESEM and XRD methods. Because In ions were not distributed uniformly in ZnO lattice, IZO and IZO_C samples show spindle-like tapered facet whereas ZnO show flat facet.

Average diameters of ZnO NSs obtained from both FESEM and TEM analysis were shown in Table 1. The average diameter of the synthesized IZO NSs using CTAB surfactant is smaller than other samples. This may due to the strong interaction between CTAB and nonpolar horizontal crystal facets of ZnO.

3.2. Optical properties

Fig. 5 shows UV-vis absorption spectra of synthesized ZnO. In IZO samples, the absorbance spectra have been broadened to the lower energy. The *Eg* values were calculated from the previous reported method [28], and are as follows: ZnO (3.12 eV), IZO (2.94 eV), IZO_C (2.87 eV), IZO_S (2.89 eV) and IZO_T (2.99 eV). It gives an evidence for the energy broadening of valence band states attributed to the doping. As the In ions incorporate into the ZnO crystals lattices, the localized band edges states form at the doped sites, resulting to red shift of UV-vis absorption bands, which indicates the appearance of a new donor level, from where the electrons can be excited to the conduction band by less energy. The highest red shift of UV-Vis absorption bands and UV-Vis absorption intensity were observed for IZO_C sample. The lowest absorption edge energy, suggested that more absorption states or defect energy bands exist in the sample [29]. The enhanced absorption related to IZO NSs probably is due to increased carrier concentration because of In doping.

It is well known that PL is a sensitive technique for determining the defects of semiconductors. Fig. 6 shows the room temperature PL spectra of the synthesized ZnO NSs, applying 325 nm excitation wavelengths. There are remarkable differences between the PL spectra of doped and undoped ZnO samples. Enhancement of the PL in respective curves was clearly observed. The most intense emission bands are related to IZO_C sample. Before doping, a broad UV emission peak ranging from 360 to 500 nm was observed due to recombination of donor-bound exciton associated with defect pairs (D_0, X) emissions [30]. In the ZnO PL spectra, the visible emission strongly depends on the crystal defects [30]. Such visible emissions can be tailored by morphology [1], changing the

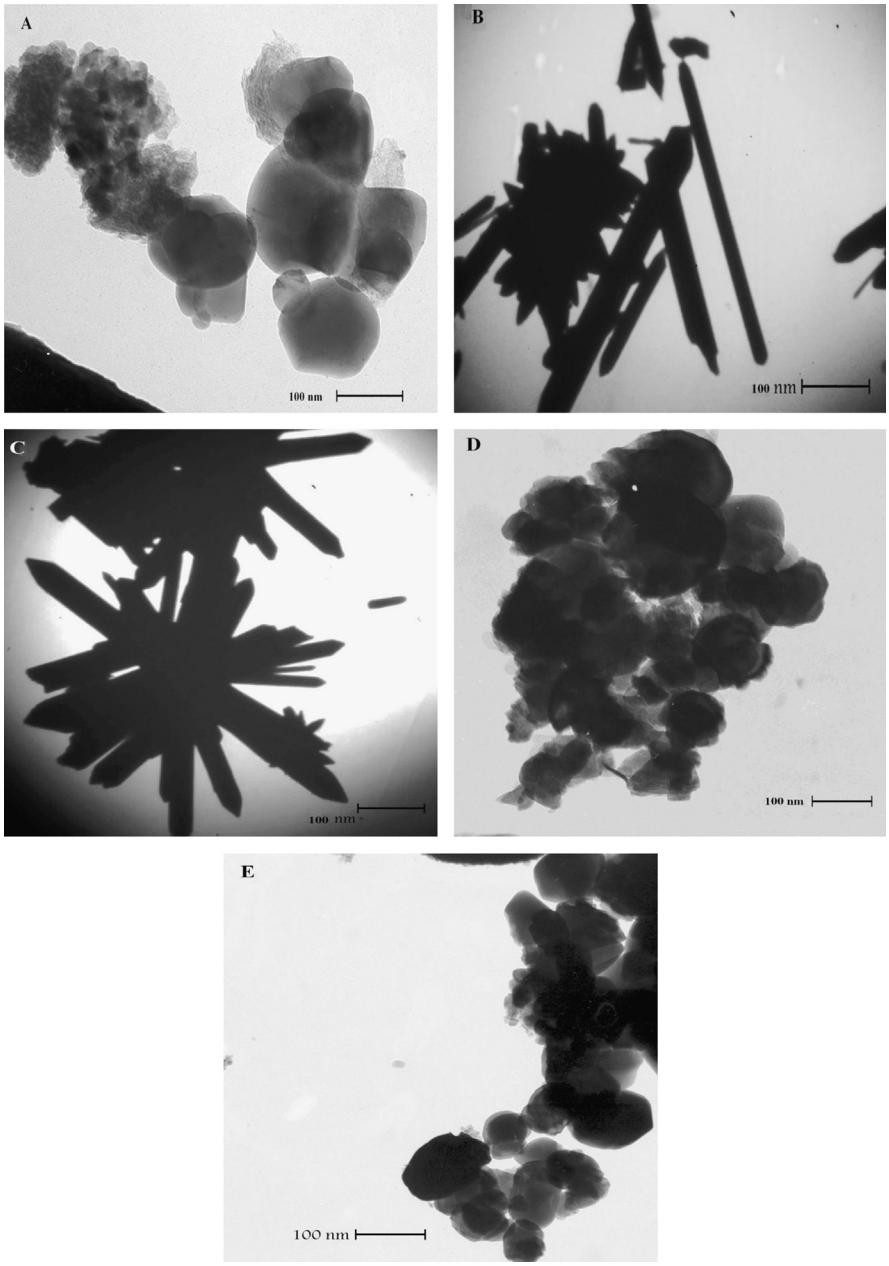

Fig. 4. TEM images of (A) ZnO, (B) IZO, (C) IZO_C, (D) IZO_S and (E) IZO_T.

Table 1
Structural and optical characteristic of synthesized ZnO nanostructures.

Sample	Morphology	(0002)/(10$\bar{1}$1) Intensity ratio	Size (nm) (TEM)	Size (nm) (FESEM)	Aspect ratio (FESEM)
ZnO	Hexagonal	0.61	81	50	–
IZO	Flower	0.76	59	64	4.8
IZO_C	Flower	0.97	49	46	10.7
IZO_S	Spherical	0.55	56	61	–
IZO_T	Polyhedral	0.66	69	72	–

annealing temperature [31], doping concentration [32] and excitation wavelength [33]. The PL spectra of synthesized IZO samples showed very intense blue–violet double broad peak centered at $\lambda \approx 395$ and 430 nm. Such emission previously was observed for undoped ZnO. It has been suggested that origins from hole trapping effect by the amine groups on the surface

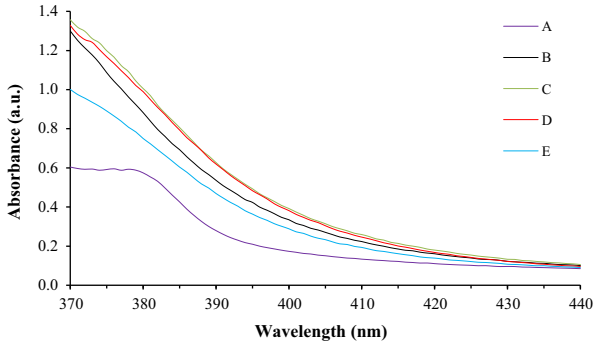

Fig. 5. UV-Vis absorption spectra of (A) ZnO, (B) IZO, (C) IZO_C, (D) IZO_S and (E) IZO_T in 370–440 wavelengths range.

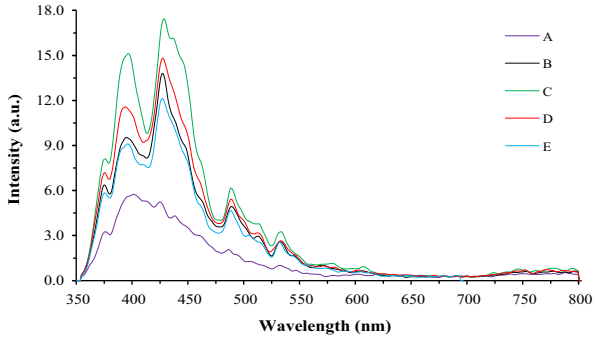

Fig. 6. Photoluminescence spectra of (A) ZnO, (B) IZO, (C) IZO_C, (D) IZO_S and (E) IZO_T.

of the ZnO [34] and also transition from conduction band to O_{Zn} level [35]. In our samples, it could be associated with a luminescent center represented as $(In_{Zn}–V_{Zn})^-$, which was formed by a doubly ionized zinc acceptor vacancy defect $(V_{Zn})^{2-}$ and an ionized impurity donor $(In_{Zn})^+$ [36]. Therefore, synthesized samples are promoted for the blue–violet light emitters and detectors and also blue lasers. Green emission observed around 530 nm wavelengths is attributed to the oxygen vacancy (V_O) [37]. Also, a visible emission band centered at 480 nm was observed that is related to interstitial Zn defects [38]. All the samples showed a weak spectrum around 610 nm related to yellow emission. The yellow emission is attributed to oxygen interstitials (O_i^-) [39].

3.3. Photocatalytic properties

Photocatalytic degradation of TCP under UV and visible irradiation was performed to investigate the PCA of synthesized ZnO NSs samples. Fig. 7 shows changes in the UV absorption intensity of TCP during different time intervals of photocatalysis process. We expect to improving PCA ZnO samples with respect to morphology, band gap energy, average particle size and vacancies results. Figs. 8 and 9 show $\ln(C_0/C)$ versus time curves of the TCP photocatalytic degradation over the ZnO, IZO, IZO_C, IZO_S and IZO_T photocatalysts under UV and visible irradiation respectively. The kinetic data of the TCP photodegradation over synthesized samples fit well to the

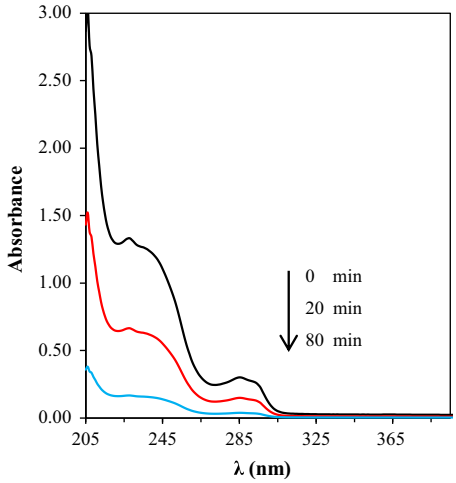

Fig. 7. UV spectral changes of TCP, recorded during the phtodegradation at different time intervals. Conditions: 0.50 g L^{-1} IZO_C, 50.00 ppm TCP, normal pH.

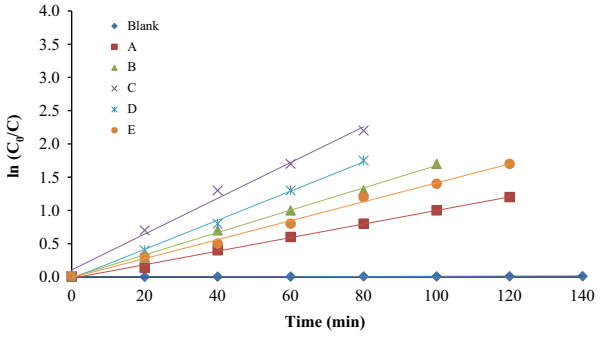

Fig. 8. Photodegradation kinetic plots with first-order linearity of $\ln(C_0/C)=f(t)$ of Blank: in the absence of UV light, (A) ZnO, (B) IZO, (C) IZO_C, (D) IZO_S and (E) IZO_T photocatalyst under UV irradiation.

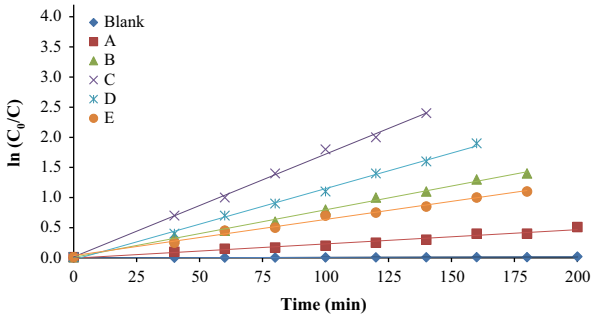

Fig. 9. Photodegradation kinetic plots with first-order linearity of $\ln(C_0/C)=f(t)$ of Blank: in the absence of visible light, (A) ZnO, (B) IZO, (C) IZO_C, (D) IZO_S and (E) IZO_T photocatalyst under visible irradiation.

pseudo first order kinetic model. Because the correlation between $\ln(C_0/C)$ and irradiation time (t) is in a good linear ($R^2 > 0.99$). The apparent photodegradation rate constants were calculated from the slopes of related curves (Table 2).

It was observed clearly that PCA of ZnO was affected by both In doping and morphology. ZnO photocatalyst showed good response to visible light, when incorporation In to ZnO

Table 2
TCP photodegradation rate constant in the presence of ZnO nanostructures under UV and visible irradiation.

Sample	K $1.0 \times 10^{-2}(\mathrm{min}^{-1})$	
	UV irradiation	Visible irradiation
ZnO	10.0	–
IZO	14.0	8.0
IZO_C	29.0	17.0
IZO_S	22.0	10.0
IZO_T	17.0	6.0

lattice. Also among all of the synthesized samples, flower-like IZO_C under both UV and visible irradiation showed highest photodegradation rate constant and so best PCA as well.

It is generally accepted that, when nanostructure semiconductor are irradiated by light with energy higher or equal to the band gap, electron in the valence band can be excited to the conduction band with the simultaneous generation of a hole (h^+) in the valence band. The photoelectron can be easily trapped by electronic acceptors like adsorbed O_2, to produce a superoxide radical anion (O_2^-); whereas the photo-induced holes can be easily trapped by electronic donors, such as organic pollutants, to further oxidation of organic pollutants [40]. As seen from kinetic data, photocatalytic rate constants of Indium doped ZnO samples under visible irradiation are close to UV irradiation one. The activation of IZO photocatalyst under visible light is mainly attributed to capability of the absorption in the visible region and band gap narrowing of ZnO modified with In doping (Fig. 5). Such occurrences can increase the efficiency of photo-generated electrons and holes formation to participate in the photocatalytic reaction.

PCA order of synthesized samples under both UV and visible irradiation are as follows: $IZO_C > IZO_S > IZO > IZO_T > ZnO$. Defects, surface area and absorption intensity of samples can explain the reasons of this sequence. One of the important cases is vacancy. The sample with higher vacancies as indicated in PL spectra (Fig. 6) shows higher rate constant too. In general, vacancies due to defects in ZnO NSs can act as the active centers to capture photo-induced electrons. This occurrence causes reduction of recombination, causing to higher activity [41]. Because photodegradation occurs on the solid–solution interface, surface area is another important factor that governs rate constant. The reachable surface area of IZO_C because of its unique morphology is much more than other products. Additional possible reason may be due to the high UV-Vis absorption intensity of IZO_C that tend to increase light-harvesting efficiency (Fig. 6).

4. Conclusions

To comprehend the role of surfactant characteristics on the crystal growth and properties of ZnO NSs, effect of surfactant charge was investigated. Results indicated that because ZnO is a polar semiconductor, surfactants through adsorption and electrostatic interaction can influence on the growth orientation. So, when using anionic surfactant like SDS, due to adsorption on the $c+$ plane, no growth along this direction was observed and when using cationic surfactant like CTAB, due to repulsion on the $c+$ plane, instability occurred, and growth along this direction increased. Also growth along all main facets was observed, when using Tritron X-100 as a nonionic surfactant. Obtained results can be utilized in the synthesis of ZnO NSs with desired growth orientation, consequently enhanced properties. ZnO NSs also was doped with In ions. Surface characteristic modification with surfactant and band gap manipulation with In dopant, enhanced remarkably optical and photocatalytic properties. Synthesized samples showed very intense blue-violet PL emission and also high PCA under visible irradiations that is very important for optical devices and chemical pollutant treatment applications respectively.

Acknowledgments

The authors are grateful for the financial support provided by Islamic Azad University, Shahreza branch. The authors also acknowledge Dr. Ali sharifzadeh for supporting this work.

References

[1] M. Rezapour, N. Talebian, Comparison of structural, optical properties and photocatalytic activity of ZnO with different morphologies: effect of synthesis methods and reaction media, Materials Chemistry and Physics 129 (2011) 249–255.
[2] L. Vayssieres, Growth of arrayed nanorods and nanowires of ZnO from aqueous solutions, Advanced Materials 15 (2003) 464–466.
[3] J. Ding, X. Yan, Q. Xue, Study on field emission and photoluminescence properties of ZnO/graphene hybrids grown on Si substrates, Materials Chemistry and Physics 133 (2012) 405–409.
[4] A.B. Patil, K.R. Patil, S.K. Pardeshi, Ecofriendly synthesis and solar photocatalytic activity of S-doped ZnO, Journal of Hazardous Material 183 (2010) 315–323.
[5] W.S. Choi, E.J. Kim, S.G. Seong, Y.S. Kim, C. Park, S.H. Hahn, Optical and structural properties of ZnO/TiO_2/ZnO multi-layers prepared via electron beam evaporation, Vacuum 83 (2009) 878–882.
[6] H. Morkoc, Ü. Özgür, Zinc Oxide, Wiley-VCH, Weinheim, 2009.
[7] F. Cai, L. Zhu, H. He, J. Li, Y. Yang, X. Chen, Z. Ye, Growth and optical properties of tetrapod-like indium-doped ZnO nanorods with a layer-structured surface, Journal of Alloys and Compounds 509 (2011) 316–320.
[8] M.N. Jung, S.H. Ha, S.J. Oh, J.E. Koo, Y.R. Cho, H.C. Lee, S.T. Lee, T.-I. Jeon, H. Makino, J.H. Chang, Field emission properties of indium-doped ZnO tetrapods, Current Applied Physics 9 (2009) 169–172.
[9] J. Yu, C. Li, S. Liu, Effect of PSS on morphology and optical properties of ZnO, Journal of Colloid and Interface Science 326 (2008) 433–438.
[10] B.A. Rozenberg, R. Tenne, Polymer-assisted fabrication of nanoparticles and nanocomposites, Progress in Polymer Science 33 (2008) 40–112.
[11] J. Liang, J. Liu, Q. Xie, S. Bai, W. Yu, Y. Qian, Hydrothermal growth and optical properties of doughnut-shaped ZnO microcrystals, Journal of Physical Chemistry B 109 (2005) 9463–9467.
[12] Z. Wang, B. Huang, X. Liu, X. Qin, X. Zhang, J. Wei, P. Wang, S. Yao, Q. Zhang, X. Jing, Photoluminescence studies from ZnO nanorods arrays synthesized by hydrothermal method with polyvinyl alcohol as surfactant, Materials Letters 62 (2008) 2637–2639.
[13] G. Colón, M.C. Hidalgo, J.A. Navío, E.P. Melián, O.G. Díaz, J.M. D. Rodríguez, Photoluminescence studies from ZnO nanorods arrays synthesized by hydrothermal method with polyvinyl alcohol as surfactant, Applied Catalysis B: Environmental 83 (2008) 30–38.

[14] N. Gopalakrishnan, L. Balakrishnan, V.S. Pavai, J. Elanchezhiyan, T. Balasubramanian, Characterization of (ZnO) (AlN)/ZnO junction for optoelectronic applications, Current Applied Physics 11 (2011) 834–837.
[15] H.-M. Cheng, W.-H. Chiu, C.-H. Lee, S.-Y. Tsai, W.-F. Hsieh, Formation of branched ZnO nanowires from solvothermal method and dye-sensitized solar cells, Journal of Physical Chemistry C 112 (2008) 16359–16364.
[16] J. Zhu, M. Zäch, Nanostructured materials for photocatalytic hydrogen production, Current Opinion in Colloid and Interface Science 14 (2009) 260–269.
[17] R. Jalal, E.K. Goharshadi, M. Abareshia, M. Moosavi, A. Yousefi, P. Nancarrow, ZnO nanofluids: green synthesis, characterization, and antibacterial activity, Materials Chemistry and Physics 121 (2010) 198–201.
[18] S. Dong, K. Xu, J. Liu, H. Cui, Photocatalytic performance of ZnO:Fe array films under sunlight irradiation, Physica B 406 (2011) 3609–3612.
[19] F. Grasset, L. Spanhel, S. Ababou-Girard, New nanocrystalline colored oxynitride thin films from Ti4+-functionalized ZnO nanocolloids, Superlattices and Microstructures 38 (2005) 300–307.
[20] C. Tai, G. Jiang, Dechlorination and destruction of 2,4,6-trichlorophenol and pentachlorophenol using hydrogen peroxide as the oxidant catalyzed by molybdate ions under basic condition, Chemosphere 59 (2005) 321–326.
[21] B.H. Hameed, Equilibrium and kinetics studies of 2,4,6-trichlorophenol adsorption onto activated clay, Colloids and Surfaces A 307 (2007) 45–52.
[22] D. Ozkaya, Particle size analysis of supported platinum catalysts by TEM, Platinum Metals Review 52 (2008) (61-61).
[23] H.P. Klug, L.E. Alexander, X-ray Diffraction Procedures, Wiley-VCH, New York, 1962.
[24] R.D. Shannon, Revised effective ionic radii and systematic studies of interatomic distances in halides and chalcogenides, Acta Crystallographica A 32 (1976) 751–756.
[25] D.G. Thomas, The diffusion and precipitation of Indium in Zinc Oxide, Journal of Physics and Chemistry of Solids 9 (1959) 31–42.
[26] V.A. Coleman, C. Jagadish, Zinc Oxide Bulk, in: C. Jagadish, S. Pearton (Eds.), Thin Films and Nanostructure, ELSEVIER, New York, 2006, pp. 2–4.
[27] K. Matsumoto, N. Saito, T. Mitate, J. Hojo, M. Inada, H. Haneda, Surface polarity determination of ZnO spherical particles synthesized via solvothermal route, Crystal Growth and Design 9 (2009) 5014–5016.
[28] P.Y. Yu, M. Cardona, in: Fundamentals of Semiconductors, Springer, Stuttgart, Germany, 2001.
[29] T. Ghoshal, S. Kar, S.J. Chaudhuri, Synthesis and optical properties of nanometer to micrometer wide hexagonal cones and columns of ZnO, Journal of Crystal Growth 293 (2006) 438–446.
[30] R.J.D. Tilley, Defects in Solids, Wiley-VCH, New Jersey, 2008.
[31] S.W. Xue, X.T. Zu, W.L. Zhou, H.X. Deng, X. Xiang, L. Zhang, H. Deng, Effects of post- thermal annealing on the optical constants of ZnO thin film, Journal of Alloys and Compounds 448 (2008) 21–26.
[32] Y.X. Liu, H.L. Zhang, X.Y. An, C.T. Gao, Z.X. Zhang, J.Y. Zhou, M. Zhou, E.Q. Xie, Effect of Al doping on the visible photoluminescence of ZnO nanofibers, Journal of Alloys and Compounds 506 (2010) 772–776.
[33] J.H. Hong, Y.F. Wang, G. He, J.X. Wang, Tuning visible emission by choosing excitation wavelength in Mg-doped ZnO/silica composites, Journal of Alloys and Compounds 506 (2010) 1–3.
[34] A. Ortíz, M. García, C. Falcony, Photoluminescent properties of indium doped zinc oxide films prepared by spray pyrolysis, Thin Solid Films 207 (1992) 175–179.
[35] M.L. Kahn, T. Cardinal, B. Bousquet, M. Monge, V. Jubera, B. Chaudret, Optical properties of zinc oxide nanoparticles and nanorods synthesized using an organometallic method, ChemPhysChem 7 (2006) 2392–2397.
[36] P.M.R. Kumar, C.S. Kartha, K.P. Vijayakumar, T. Abe, Y. Kashiwaba, F. Singh, D.K. Avasthi, On the properties of indium doped ZnO thin films, Semiconductor Science and Technology 20 (2005) 120–126.
[37] K. Vanheusden, W.L. Warren, C.H. Seager, D.R. Tallant, J.A. Voigt, B. E. Gnade, Mechanisms behind green photoluminescence in ZnO phosphor powders, Journal of Applied Physics 79 (1996) 7983–7990.
[38] X. Peng, H. Zang, Z. Wang, J. Xu, Y. Wang, Blue–violet luminescence double peak of In- doped films prepared by radio frequency sputtering, Journal of Luminescence 128 (2008) 328–332.
[39] X.L. Wu, G.G. Siu, C.L. Fu, H.C. Ong, Photoluminescence and cathodoluminescence studies of stoichiometric and oxygen-deficient ZnO films, Applied Physics Letters 78 (2001) 2285–2287.
[40] S. Ahmed, M.G. Rasul, W.N. Martens, R. Brown, M.A. Hashib, Heterogeneous photocatalytic degradation of phenols in wastewater: a review on current status and developments, Desalination 261 (2010) 3–18.
[41] L.H. Quang, L.S. Kuan, G.G.K. Liang, Structural and electrical properties of single crystal indium doped ZnO films synthesized by low temperature solution method, Journal of Crystal Growth 312 (2010) 437–442.